Identification of an immune-related eRNA prognostic signature for clear cell renal cell carcinoma

Yang Lv[1,*], Lili Niu[2,3,*], Qiang Li[1,4], Wenchuan Shao[5], Xinghan Yan[5], Yang Li[6], Yulin Yue[7], Hongqi Chen[1]

[1]Department of Urology, The Affiliated Jiangsu Shengze Hospital of Nanjing Medical University, Suzhou 215228, China
[2]Central Laboratory, First Affiliated Hospital, Institute (College) of Integrative Medicine, Dalian Medical University, Dalian 116021, China
[3]Department of Pharmacy, Shanghai Pudong Hospital, Fudan University Pudong Medical Center, Shanghai 201399, China
[4]Department of Urology, The First Affiliated Hospital of Soochow University, Suzhou, China
[5]Department of Urology, The State Key Lab of Reproductive, The First Affiliated Hospital of Nanjing Medical University, Nanjing 210029, China
[6]Department of Urology, Shanghai Pudong Hospital, Fudan University Pudong Medical Center, Shanghai 201399, China
[7]Department of Clinical Laboratory, Children's Hospital of Nanjing Medical University, Nanjing, China
[*]Equal contribution

Correspondence to: Hongqi Chen, Yulin Yue, Yang Li; **email:** hjsszchq@163.com, https://orcid.org/0009-0006-9895-3441; yueyulin@njmu.edu.cn; 15821477378@163.com, https://orcid.org/0009-0001-2203-6800
Keywords: non-coding RNA, enhancer RNA, immune signature, tumor microenvironment, clear cell renal cell carcinoma
Received: August 15, 2023   **Accepted:** December 1, 2023   **Published:** January 29, 2024

ABSTRACT

Background: Immune-related enhancer RNAs (eRNAs) have garnered significant attention in cancer metabolism research, yet their specific roles in ccRCC have remained elusive.
Methods: We retrieved eRNA expression profiles from TCGA database and identified immune-related eRNAs (IREs) by assessing their co-expression with immune genes. Utilizing consensus clustering, we organized these IREs into two distinct clusters. The construction of an IREs signature was accomplished through the LASSO and multivariate Cox analysis. Furthermore, we performed Cell Counting Kit-8 and clonogenic assays to assess changes in the proliferative capacity of Caki-1 and 769-P cells.
Results: The existence of two clusters of immune-related eRNAs in ccRCC, each with distinctive prognostic and immunological attributes. Cluster B exhibited immunosuppressive properties and displayed a positive correlation with immunosuppressive cells. Functional enrichment analysis unveiled their involvement in several tumor-promoting pathways, metabolic pathways and immune pathways. The IREs signature demonstrated its potential to accurately predict patient immune and prognostic characteristics. AC003092.1, an eRNA strongly associated with patient survival, emerged as a potential oncogene significantly linked to adverse prognosis and the presence of immunosuppressive cells and checkpoints in ccRCC patients. Notably, AC003092.1 displayed marked upregulation in ccRCC tissues and cell lines, and its knockdown substantially inhibited the proliferation of Caki-1 and 769-P cells.

Conclusion: We established a robust predictive model that played a vital role in determining the prognosis, clinicopathological characteristics and immune cell infiltration patterns of ccRCC patients. IRE, particularly AC003092.1, which was strongly associated with survival, hold promise as novel immunotherapeutic targets for ccRCC.

INTRODUCTION

Renal cell carcinoma (RCC) is an intricate malignancy that originates from epithelial cells, with renal clear cell carcinoma (ccRCC) being the most common subtype [1]. The incidence and mortality of ccRCC have been steadily increasing, now accounting for approximately two to three percent of adult malignancies [2, 3]. Given its insensitivity to targeted and immunosuppressive agents, surgical intervention remains the primary and most effective treatment modality [4]. Despite significant advancements in early screening and diagnosis, approximately 30% of patients present with metastases at the time of diagnosis and about 25% develop metastases following surgical treatment [5, 6]. Consequently, the urgency lies in the quest for an effective prognostic signature and potential biomarkers to enhance the treatment of ccRCC patients.

RCC represents a prototypical immunogenic tumor that predominantly relies on inducing immunosuppressive cells, such as regulatory T cells, myeloid-derived suppressor cells, and macrophages, to create an immunosuppressive microenvironment [7]. The immune microenvironment has a dual role—it can inhibit tumor growth but also facilitate tumor progression by altering tumor immunogenicity or immunosuppression status [8]. Within the RCC tumor microenvironment, immunosuppressive cells may disrupt immune surveillance, ultimately leading to tumor immune evasion or escape [9]. RCC achieves this by upregulating the expression of immunosuppressive checkpoints, thereby inhibiting the activity of effector T cells and antigen-presenting cells, thus promoting tumor metastasis [10]. Consequently, it becomes imperative to explore the immune-related prognostic model for ccRCC.

Long noncoding RNAs (lncRNAs) are RNA transcripts exceeding 200 nucleotides in length that do not encode proteins; they are distributed widely in both the cytosol and nucleus [11, 12]. A growing body of evidence underscores the pivotal role of lncRNAs in regulating gene expression, translation and tumor progression [13, 14]. eRNAs are a class of RNA transcribed from enhancer regions on the genome, and they are found abundantly in most human cells and tissues [15, 16]. There is mounting evidence linking eRNA transcriptional levels to enhancer activity, implicating

them in gene transcriptional regulation and their close association with tumor proliferation and metastasis [17, 18]. Moreover, eRNAs may contribute to tumor progression by regulating nuclear histone structure or interacting with transcriptional regulators [19, 20]. In human cells, eRNA participate in various signal transduction pathways and influence the construction of immune microenvironment by mediating the activation of target genes, thus underscoring the clinical significance of eRNA-targeted therapy [17]. Although immune-related eRNAs (IREs) play a substantial role in gene transcriptional control, their underlying mechanisms in ccRCC remain elusive.

In this study, we conducted a comprehensive evaluation of the prognostic characteristics of IREs in ccRCC. Notably, we established two distinct clusters of IREs, each with unique prognostic and immune characteristics. Additionally, we developed an IREs prognostic model that effectively predicts the survival rates of ccRCC patients. AC003092.1, a key player in the regulation of the tumor immune microenvironment, holds promise in guiding the development of immunotherapies for ccRCC.

METHODS

Clinical data acquisition and extraction

Gene expression profiles and clinical data of ccRCC patients were sourced from The Cancer Genome Atlas (TCGA). The dataset comprised 538 cases of ccRCC tissues and 72 cases of normal tissues. For validation, gene expression data for ccRCC were obtained from ArrayExpress (https://www.ebi.ac.uk/arrayexpress) and the International Cancer Genome Consortium (ICGC) (https://icgc.org). The ArrayExpress dataset has the accession number E-MTAB-1980, including 106 cases with follow-up information. The ICGC dataset is labeled as RECA-EU and encompasses 91 cases with follow-up data.

Identification of immune-related eRNAs

To identify immune-related eRNAs (IREs), we gathered immune-related genes from the Molecular Signatures Database (MSigDB) categories IMMUNE_RESPONSE and IMMUNE_SYSTEM_PROCESS. We determined eRNAs transcribed from active tissue-specific

enhancers and predicted their target genes using the Predicted Gene and enhancer Specific Tissue Interaction (PresSTIGE) method [21, 22]. The Pearson correlation analysis was employed to screen for IREs, with the criterion being a |Pearson correlation coefficient| >0.4 and $p < 0.001$. AC003092.1 expression in ccRCC was assessed using quantitative real-time PCR (qRT-PCR). The primers for AC003092.1 were as follows: Forward: TTAGCAGCAAACCCAGAAC; Reverse: TGCTGAGGATACATGACGAA. The primers for GAPDH were: Forward: GAGGTGATA GCATTGCTTTCG; Reverse: CAAGTCAGTGTACA GGTAAGC.

Construction of immune-related eRNAs clusters and bioinformatics analysis

We conducted univariate Cox regression analysis to identify IREs associated with prognosis. To investigate the function of IREs in ccRCC, we employed the "Consensus ClusterPlus" package for patient classification. Kaplan-Meier (KM) survival curves were generated to assess survival differences among these clusters. To further analyze biological pathways, we screened differential expression genes (DEGs) based on the criteria |log 2 (fold change FC)| >2 and adjusted *P*-value < 0.001. We used Gene Ontology (GO) and Kyoto Encyclopedia of Genes and Genomes (KEGG) for the analysis of molecular roles and associated biological processes of DEGs. Additionally, Gene Set Variation Analysis (GSVA) enrichment analyses were conducted to evaluate pathway enrichment using the R package "GSVA" and "c2.cp.kegg.v7.4.symbols" from the MSigDB. The gene set "c2.cp.kegg.v7.4. symbols" is a commonly used gene set from the MSigDB database, which aggregates information related to gene pathways.

Analysis of immune characters in immune-related eRNAs clusters

We employed single-sample Gene Set Enrichment Analysis (ssGSEA) to calculate the scores of immune-infiltrating cells and immune-related pathways in individual samples. The "ESTIMATE" R package was used to estimate tumor purity, stromal and immune scores in the tumor microenvironment of ccRCC samples.

Establishment of immune-related eRNAs signature

Using the expression profile of prognostic IREs, we utilized the Least absolute shrinkage and selection operator (LASSO) regression analysis and multivariate Cox regression analysis to screen key genes and construct the IREs prognostic model. The following formula was used to calculate the risk score for each sample:

$$\text{Riskscore} = \sum_{l}^{i}(Coefi \times Gen\exp i)$$

Here, "Coef" represents non-zero regression coefficients determined through multivariate Cox regression analysis, and "Genexp" is the expression values of genes from IREs prognostic model. Patients were divided equally into high - and low-risk groups according to the median riskscore. KM survival curves were constructed to compare survival differences between these groups. Univariate and multivariate Cox regression analyses were conducted to assess the independence of riskscore and various clinico-pathological features including age, gender, histological grade, pathological stage, and TMN stage.

Prognostic features of immune-related eRNAs signature

To analyze the correlation between riskscore and clinicopathological variables, we further assessed differences in the riskscore among various clinico-pathological variables. Chi-square tests were employed to evaluate differences in the distribution of clinico-pathological variables between the high - and low-risk groups. Additionally, KM survival curves were used to analyze differences in survival between the high - and low-risk groups within different clinical phenotypes.

Identification of the key eRNA in ccRCC

Based on the significant IREs expression profiles identified through univariate Cox analysis, patients were divided into high and low expression groups, and survival characteristics in ccRCC were analyzed further. Co-expression analysis was used to assess the correlation between IREs expression levels and their predicted target genes. IREs were included if they demonstrated a significant association with overall survival (OS) (KM log rank $p < 0.05$) and a significant association with predicted target genes (|r| >0.4 and $p < 0.001$). Key IREs, most relevant for survival according to log rank *p*-values, were selected for further analysis. The prognostic features of key IREs and their correlation with clinicopathological features were also investigated.

Cell culture and plasmid construction

We obtained two human ccRCC cell lines (Caki-1 and 769-P) and a human renal proximal tubular epithelial HK2 cell line (HRPTEpiC) that were purchased from the cell bank of the Chinese Academy of Sciences (Shanghai, China). All cells were cultured in RPMI 1640

medium (Thermo Fisher Scientific, Inc., Waltham, MA, USA) supplemented with 10% fetal bovine serum (FBS; Thermo Fisher Scientific, Inc.) at a constant temperature of 37°C in a humidified atmosphere containing 5% CO_2.

To silence AC003092.1, two siRNAs were transfected into Caki-1 and 769-P cells using Lipofectamine 3000 (Thermo Fisher Scientific, Inc.), following the manufacturer's instructions. The sequences used for siRNA-1 were: Sense: GUAAUCCAGCGAAUCUGGA; Antisense: UCCAGAUUCGCUGGAUUAC; siRNA-2: Sense: CAGCAAUCAACAUAAUCAA; Antisense: UUGAUUAUGUUGAUUGCUG.

Cell counting kit-8 (CCK8) assay

Briefly, Caki-1 and 769-P cells, after various interventions, were incubated in 96-well plates (2×10^3) with 200 µL of culture medium at 37°C with 5% CO_2. On days one, two, three, four and five, 20 µL CCK-8 solution was added into each well, and incubation was carried out for two hours. Absorbance was measured at an optical density of 450 nm using a Microplate reader (Bio-Rad Laboratories Inc., Hercules, CA, USA). Experiments were conducted in triplicate.

Cell growth assay and clonal formation assay

For the Cell Growth Assay, cell viability was assessed in accordance with the manufacturer's instructions. Cells were initially seeded at a density of 2×10^3 cells per well in 96-well plates and evaluated at 0, 24, 48, 72, and 96 hours by the Cell Counting Kit-8 (Beyotime, Shanghai, China) and the Synergy H1 microplate reader (BioTek, Winooski, VT, USA) at 450 nm. In the case of the Clonal Formation Assay, after transfection and selection, 200 cells were distributed in 6-well plates in triplicate and incubated for 14 days. Subsequently, the cells were fixed with 10% ice-cold methanol and stained with 0.5% crystal violet solution. Colonies consisting more than 50 cells per colony were counted, and independent experiments were conducted in triplicate.

Data availability statement

All data used in this work can be acquired from (TCGA, (https://portal.gdc.cancer.gov/), GEO (https://www.ncbi.nlm.nih.gov/geo/).

RESULTS

Establishment of immune-related eRNAs clusters

The Supplementary Figure 1 displayed the entire process of this study. Initially, we employed univariate Cox regression analysis on a set of 146 IREs,

meticulously selecting 64 IREs linked to prognosis based on the stringent criterion of $P < 0.01$ (Supplementary Table 1). Subsequently, utilizing the expression profile of these prognostic IREs, we categorized patients into two distinct clusters, denoted as cluster A and cluster B, employing the Consensus ClusterPlus package (Figure 1A). KM survival curve analysis revealed a notable difference in survival between these clusters, with cluster B associated with a less favorable prognosis (Figure 1B). Furthermore, principal component analysis (PCA) illustrates the distinction between cluster A and cluster B (Figure 1C). The heatmap was generated to display the distribution of the IREs' expression and clinicopathological variables, highlighting the higher expression of IREs in cluster A (Figure 1D). Additionally, we employed GSVA to assess differences in biological pathways between the two clusters. The results indicated enrichment of multiple metabolic pathways, including fatty acid metabolism, glycerolipid metabolism and beta alanine metabolism in cluster A, while cluster B exhibited enrichment in multiple pro-cancer pathways, such as the P53 signaling pathway (Figure 1E).

Furthermore, we screened 2619 DEGs for further analysis based on the criteria of |log 2 (fold change FC)| >2 and adjusted P-value < 0.001. These DEGs were categorized into Biological Process (BP), Cellular Component (CC), and Molecular Function (MF) groups. In the BP group, genes were primarily enriched in processes related to neutrophil activation, response to oxidative stress, and regulation of angiogenesis. In the CC group, genes were concentrated in focal adhesion, cell–substrate adherens junctions, and cell–substrate junctions. In the MF group, genes were significantly enriched in functions related to cell adhesion molecule binding, cadherin binding, and growth factor binding (Figure 1F). The KEGG enrichment analysis highlighted the significant enrichment of DEGs in multiple pro-cancer pathways, renal cell carcinoma, metabolic pathways and hypoxia related pathways (Figure 1G).

Identification immune characteristics of immune-related eRNAs clusters

To investigate the immune characteristics of the Immune-Related eRNAs clusters, we utilized the ssGSEA algorithm to calculate the immunosuppressive cell infiltration score in individual ccRCC samples. Notably, immunosuppressive cells, including Myeloid-Derived Suppressor Cells (MDSCs), Macrophages, and Regulatory T cells, exhibited significant overexpression in cluster B (Figure 2A–2C). Furthermore, we applied the ESTIMATE algorithm to calculate the estimated score, immune score, stromal score and tumor purity of

the tumor microenvironment. Our findings indicated that estimated score, immune score, and stromal score were significantly higher in cluster B, while tumor purity was significantly lower in cluster B (Figure 2D–2G). We further analyzed the differential expression of immune function pathways among the different clusters, revealing that pathways such as Antigen-Presenting Cell (APC) co-stimulation, Cytokine Receptor Regulation (CCR), Checkpoint Pathways, and Parainflammation were significant higher in the cluster B (Figure 2H).
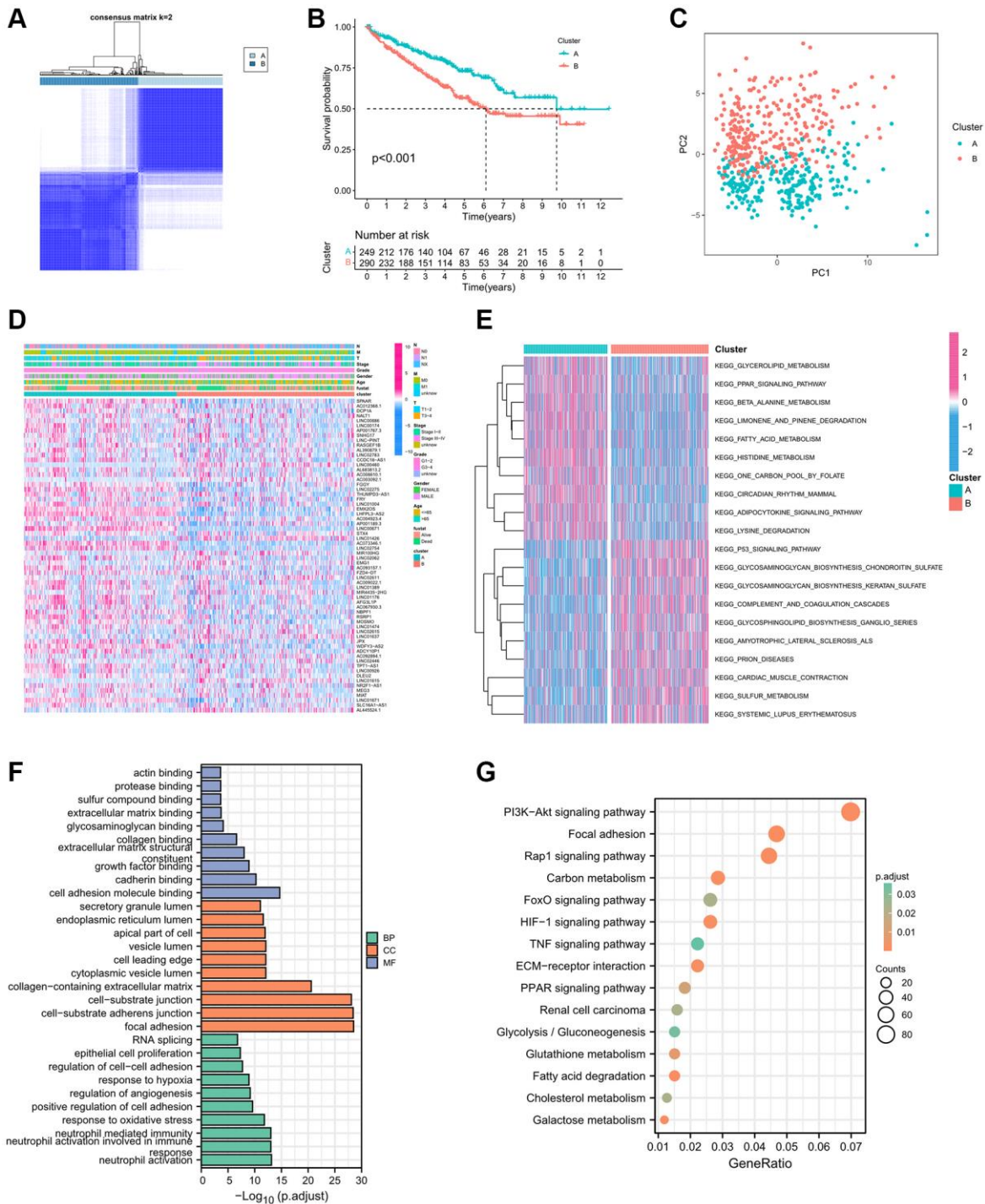
Figure 1. Establishment biological analysis of immune-related eRNAs clusters. (**A**) Sample distribution of 2 immune-related eRNAs clusters; (**B**) KM curve showing the survival differences between clusters; (**C**) PCA showing the trend of sample distribution between 2 clusters. (**D**) The heatmap presenting the distribution of immune-related eRNAs and clinical phenotype; (**E**) The heatmap showing the results of GSVA enrichment analysis between 2 clusters. Pink represented activated pathways; blue represented inhibited pathways. (**F**) GO analysis of differential genes between clusters. (**G**) KEGG analysis of intersection genes of differential genes between clusters.

Development of immune-related eRNAs signature

In the process of developing the IREs signature, we initially employed Lasso regression analysis to further refine our selection from the initial 64 prognostic IREs, ultimately identifying 33 prognostic IREs (Figure 3A, 3B).

Subsequently, we utilized multivariate Cox regression analysis and identified the 15 most relevant IREs with the lowest Akaike information criterion (AIC) value, which were then used to construct the IREs signature (Figure 3C). Based on the median of riskscore, ccRCC patients were equally divided into high and
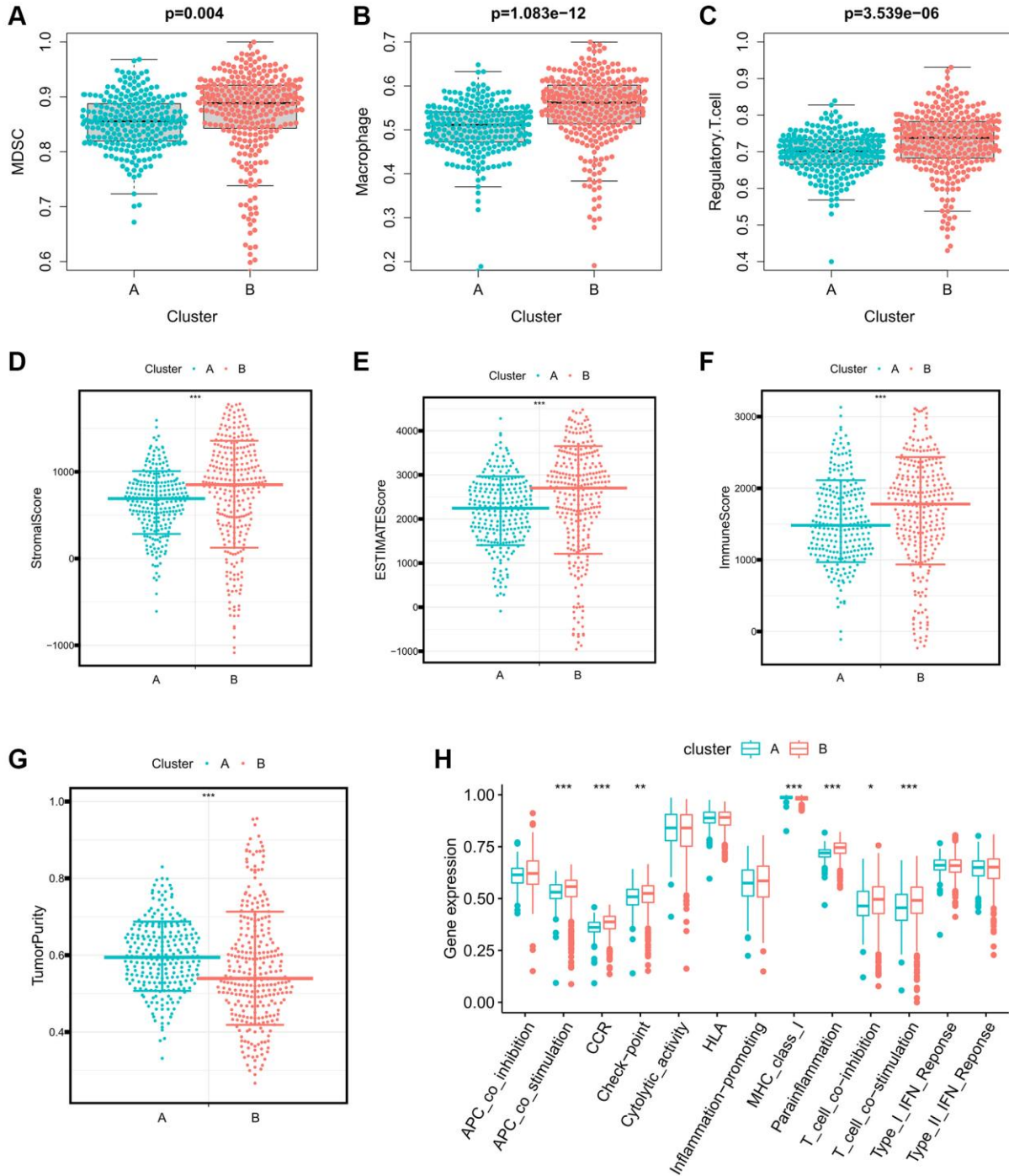

Figure 2. Differences in immune characteristics between immune-related eRNAs clusters. (**A**–**C**) Differences in expression of immunosuppressive cells between 2 clusters (**A**: MDSC; **B**: Macrophage; **C**: Regulatory.T.cell); (**D**–**G**) Differences in the expression of tumor microenvironment score between 2 clusters (**A**: StromalScore; **B**: ESTIMATEScore; **C**: ImmuneScore; **D**: TumorPurity); (**H**) Differences in expression of immune function pathways between 2 clusters.

low risk groups. The riskscore exhibited an inverse association with patient survival in the ccRCC sample, clearly depicted in Figure 3D. Furthermore, the heatmap illustrated the distribution of the modeled genes and clinicopathological variables (Figure 3E). The KM survival curve analysis highlighted that patients in the high-risk group had a significantly worse prognosis compared to those in the low-risk group (Figure 3F). We assessed the predictive accuracy of the riskscore by calculating the Area Under the Curve (AUC) for one-year, two-year, and tree-year risk scores, resulting in AUC values of 0.809, 0.783, and 0.781, respectively. This demonstrated that the riskscore was effective in accurately predicting patient prognosis (Figure 3G). To further validate the independence and accuracy of the riskscore in predicting patient prognosis, we performed univariate and multivariate independent prognostic analyses, considering the riskscore and clinico-pathological variables. The univariate independent prognostic analysis demonstrated that age, grade, stage, TMN stage, and riskscore significantly impacted OS (Figure 3H). Meanwhile, the multivariate independent prognostic analysis confirmed that the riskscore remained an independent prognostic indicator for OS (HR: 1.100, 95%CI: 1.057−1.146, p-value < 0.001) (Figure 3I).

Identification of clinical characteristic of immune-related eRNAs signature

To further investigate the relationship between riskscore and clinicopathological variables, we initially examined
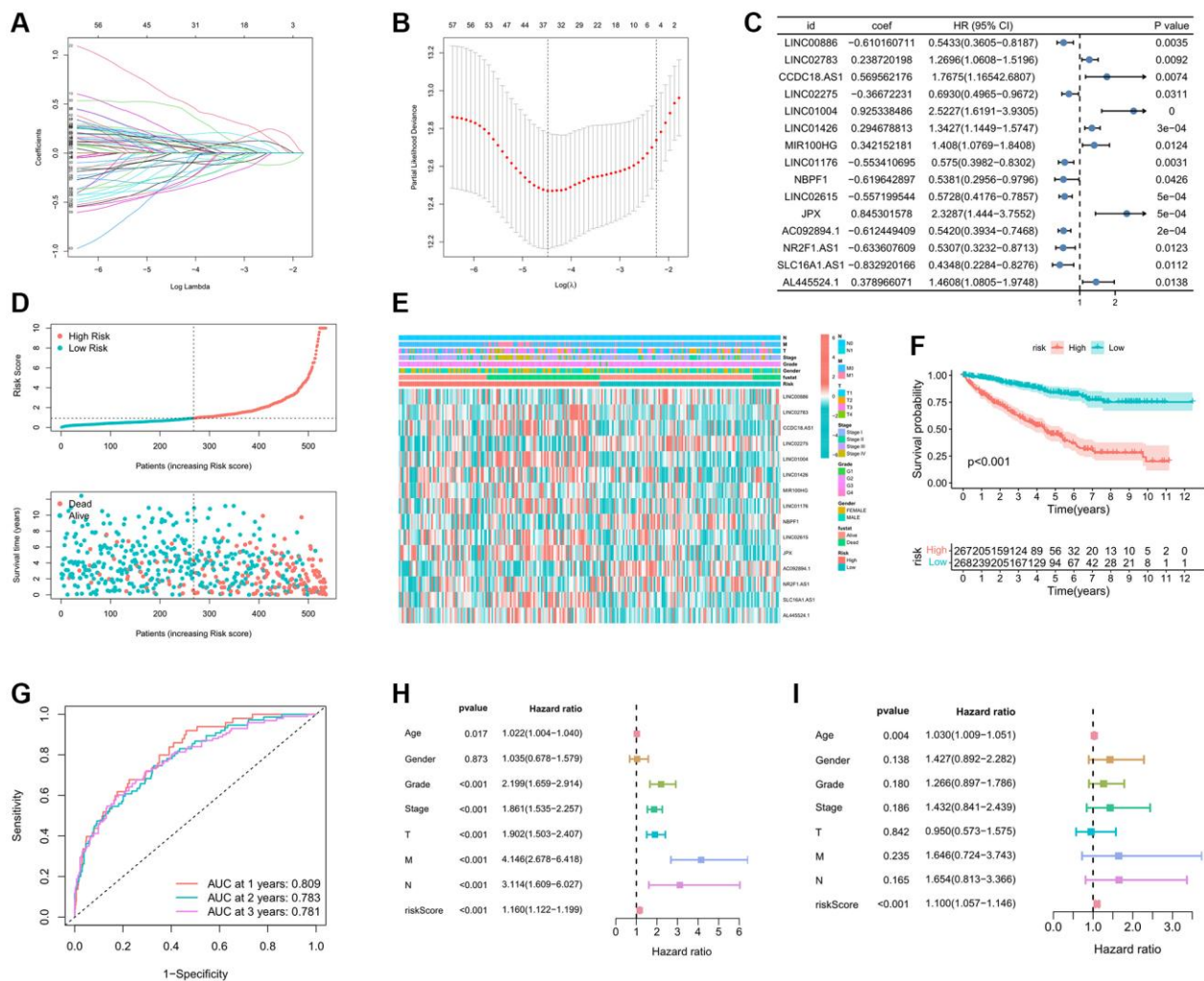

Figure 3. Establishment prognostic analysis of immune-related eRNAs signature. (**A**) LASSO coefficient profiles of the expression of prognostic immune-related eRNAs. (**B**) Selection of the penalty parameter (λ) in the LASSO model via 10-fold cross-validation. (**C**) Results of immune-related eRNAs multivariate analysis; (**D**) Relationship between the survival status/immune-related eRNAs signature rank and survival time (years)/immune-related eRNAs signature rank; (**E**) Distribution of immune-related eRNAs expression and clinical phenotype between high and low risk groups; (**F**) KM curve showing the survival differences between high and low risk groups; (**G**) Time-dependent ROC curve for OS of the riskscore. The AUC was assessed at 1, 2 and 3 years; The univariate (**H**) and multivariate (**I**) Cox regression analysis of riskscore, age, gender, grade, stage, and TMN.

the differences in riskscore expression among various clinicopathological variables. Interestingly, significant variations in riskscore expression were observed among different IREs clusters, histological grade, pathological stage, and TNM stage (Figure 4A). Notably, a trend was observed where more advanced clinical phenotypes were associated with higher riskscores. Additionally, we conducted chi-square tests to evaluate differences in the distribution of clinicopathological variables between high and low-risk groups. The results revealed that the high-risk group had a higher proportion of advanced clinicopathological variables, and these differences were statistically significant, except for the N stage (Figure 4B). Furthermore, through an analysis of the differences in survival between the high and low risk groups within various clinical phenotypes, we observed that the high-risk group consistently exhibited a poorer prognosis across all clinical phenotypes, with statistically significant differences (Figure 4C).

Identification of prognostic characteristics of the key eRNA---AC003092.1

As detailed in Supplementary Table 2, AC003092.1 emerged as the eRNA most strongly associated with survival, with a notably positive correlation to its predicted target, TFPI2. Subsequently, patients were evenly stratified into high and low AC003092.1 expression groups based on the median expression of AC003092.1 in ccRCC. Differences in survival outcomes, including OS, disease specific survival (DSS), and progress free interval (PFI) were assessed between these two groups. The analysis revealed that the high AC003092.1 group exhibited an adverse prognosis in OS, DSS, and PFI compared to the low AC003092.1 group, and these differences held statistical significance (Figure 5A–5C). Furthermore, when comparing AC003092.1 expression levels between ccRCC and adjacent tissues, AC003092.1 was
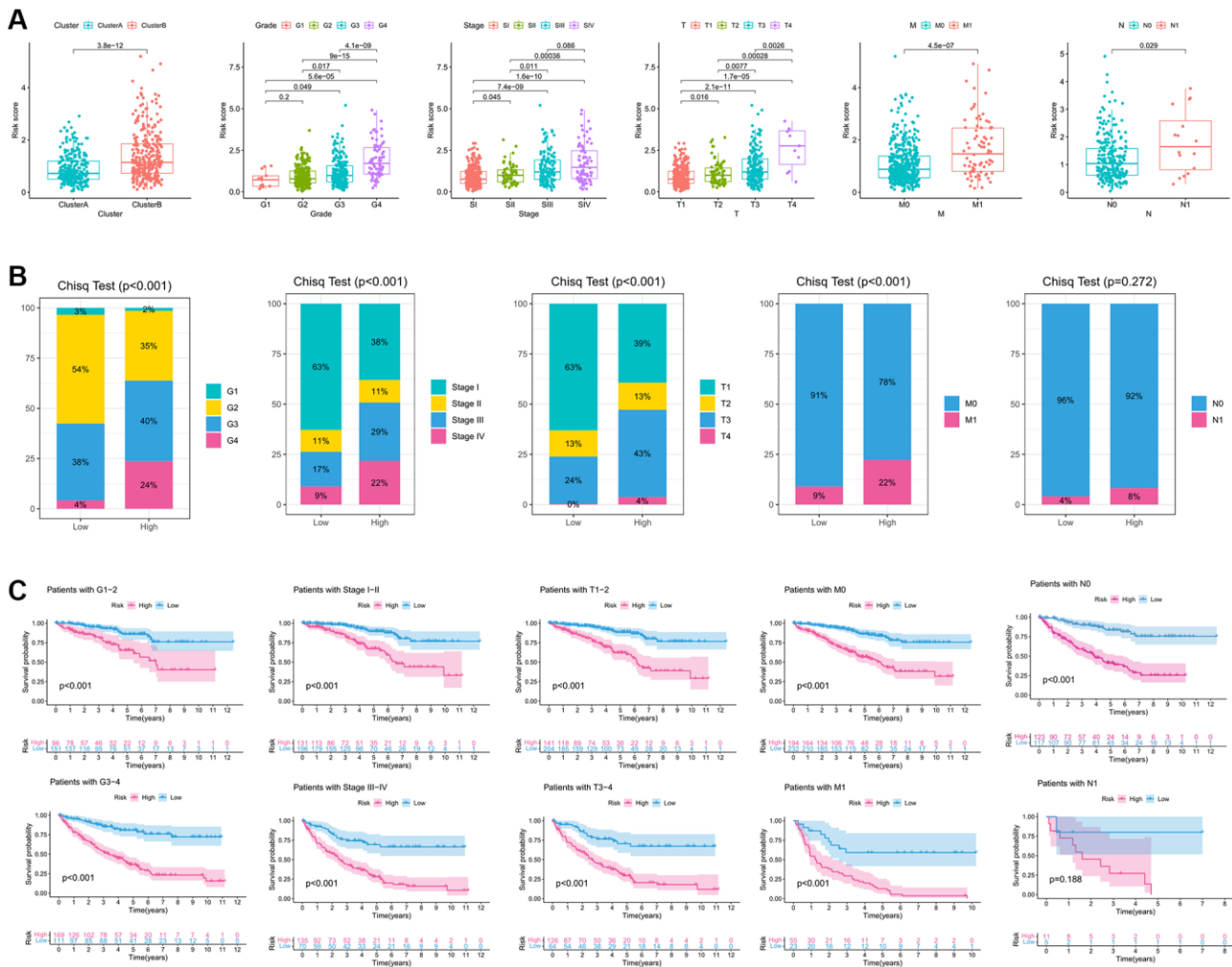

Figure 4. Clinicopathological characteristic of the immune-related eRNAs signature. (**A**). Differences in the expression of riskscore in various clinicopathological stages; (**B**) Differences in the proportion of different clinicopathological stages between high and low riskscore groups. (**C**) KM survival curve showing the survival differences between high and low score groups in different clinicopathological stages.

found to be significantly upregulated in ccRCC (Figure 5D). The KM survival curve demonstrated that the high TFPI2 group was associated with a less favorable prognosis for ccRCC patients (Figure 5E). Additionally, we delved into the relationship between AC003092.1 expression and clinicopathological characteristics in ccRCC, revealing a significant positive correlation between the expression level of AC003092.1 and several clinicopathological features, including patient status, histological grade, pathological stage, and TNM stage (Figure 5F–5J). Furthermore, external validation sets, E-MTAB-1980 and ICGC, corroborated the association of AC003092.1 expression with a poor prognosis (Figure 5K, 5L).
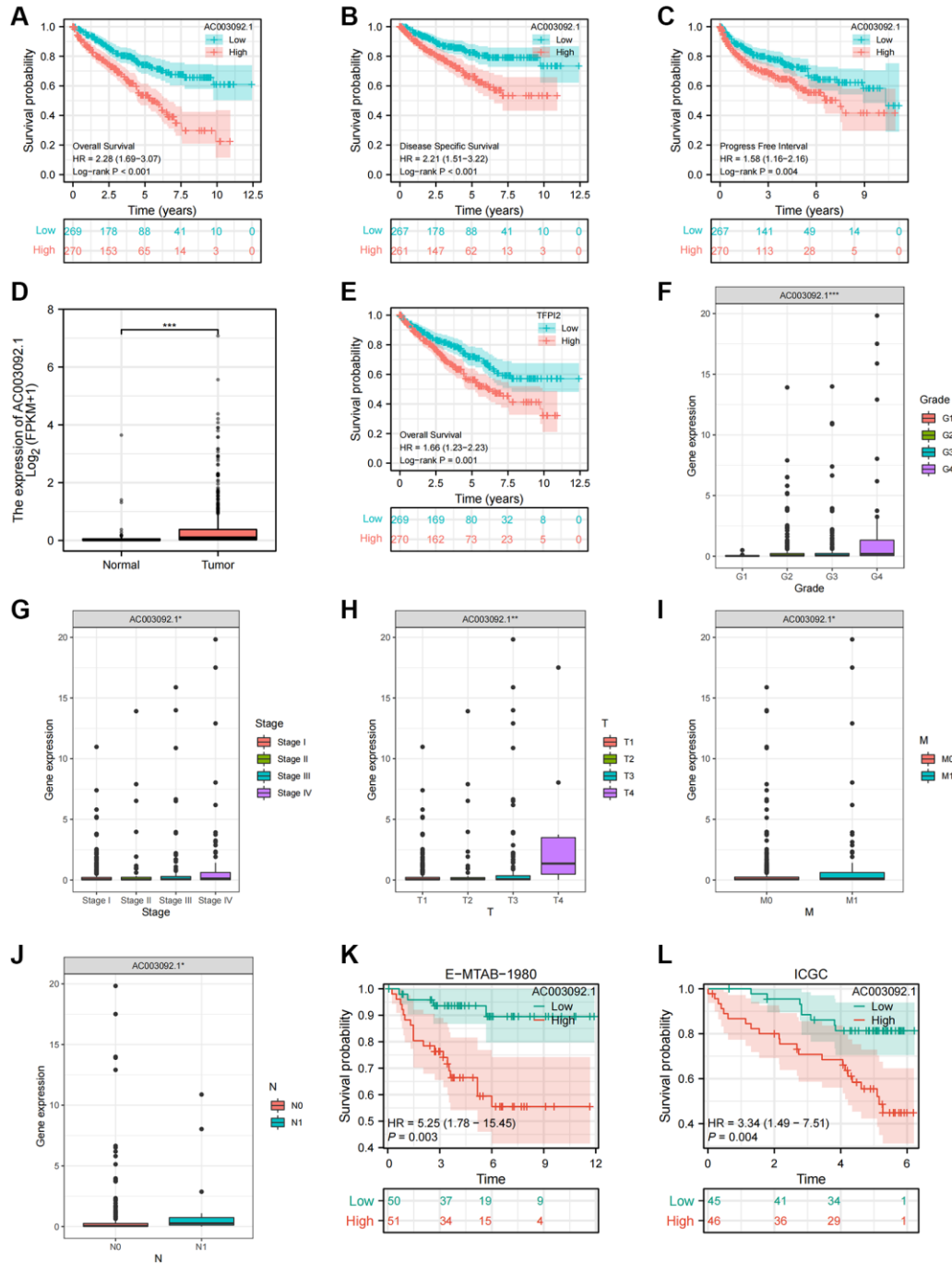

Figure 5. Clinical and prognostic characteristics of AC003092.1 in ccRCC. (A–C) KM survival curve showing the survival differences between high and low AC003092.1 groups (**A**: OS; **B**: DSS; **C**: PFI); (**D**) Difference of AC003092.1 mRNA expression between ccRCC and adjacent tissues; (**E**) KM survival curve showing the survival differences between high and low TFPI2 groups; (**F–J**) Differences of AC003092.1 expression in different clinicopathological variables (**F**: Grade; **G**: Stage; **H**: T stage; **I**: M stage; **J**: N stage); (**K, L**) KM survival curve showing the survival differences between high and low AC003092.1 groups in the E-MTAB-1980 and ICGC datasets.

Identification of immune characteristics of the key eRNA---AC003092.1

To gain deeper insights into the role of AC003092.1 in the tumor microenvironment, we explored the correlation between AC003092.1 and immune cells as well as tumor microenvironment scores. A heatmap highlighted that immunoinfiltrating cells and tumor microenvironment score were notably upregulated in the high AC003092.1 group (Figure 6A). Figure 6B presented the correlation between AC003092.1 and immune infiltrating cells, revealing a significantly
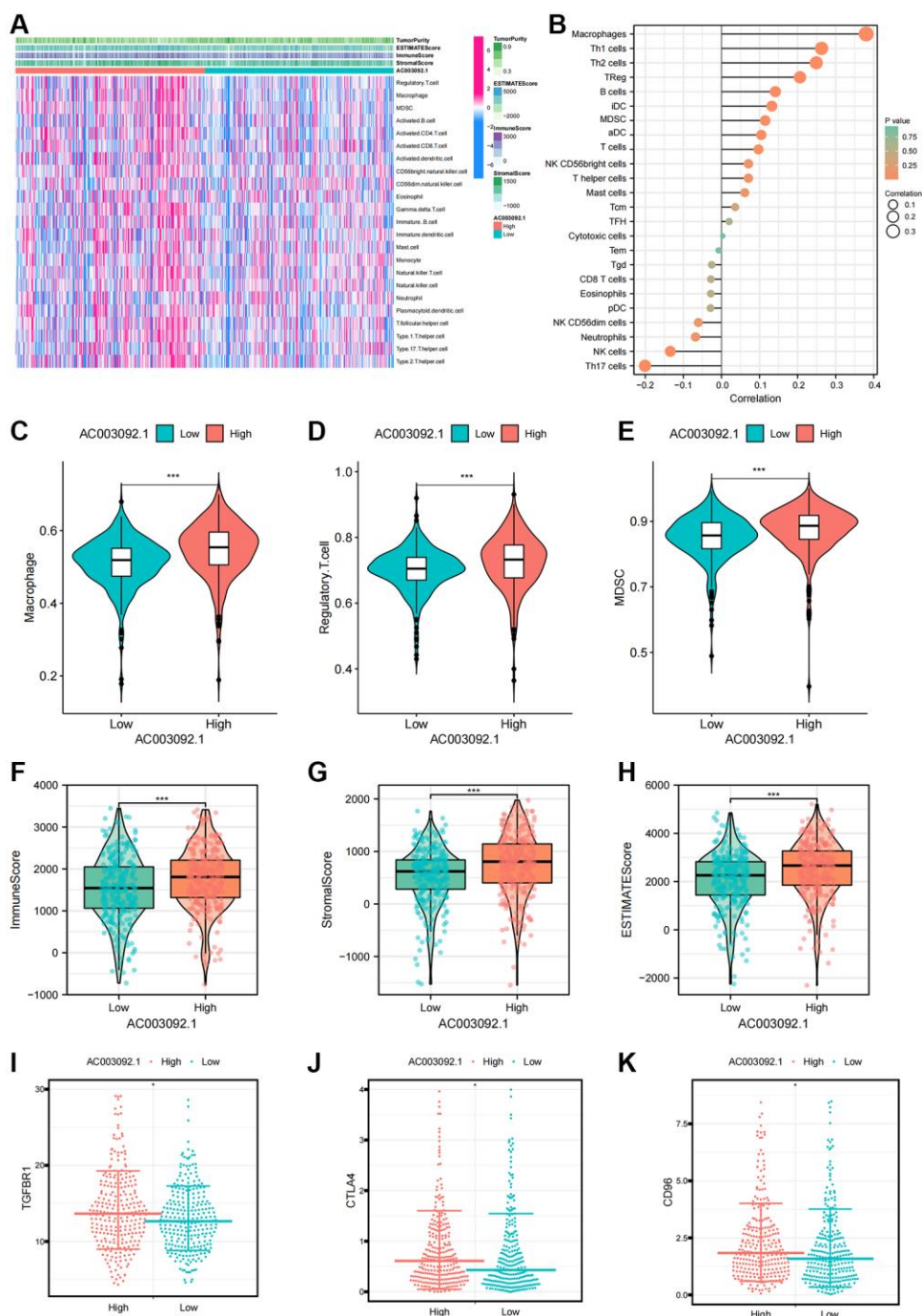

Figure 6. Immune characteristics of AC003092.1 in ccRCC. (**A**) Distribution of immune infiltrating cells and tumor microenvironment scores in high and low AC003092.1 expression groups; (**B**) Correlation between immunoinfiltrating cells and AC003092.1 expression profiles. (**C–E**) Differences in immunosuppressive cell expression between high and low AC003092.1 groups (**C**: Macrophage; **D**: Regulatory.T.cell; **E**: MDSC); (**F–H**) Differences in tumor microenvironment scores between high and low AC003092.1 groups (**F**: ImmuneScore; **G**: StromalScore; **H**: ESTIMATEScore); (**I–K**) Differences in immune suppression checkpoints between high and low AC003092.1 groups (**I**: TGFBR1; **J**: CTLA4; **K**: CD96).

positively correlation with immunosuppressive cells (MDSC, Macrophage and Regulatory.T.cell) and a negative correlation with NK cells and neutrophils. This analysis was complemented by a noticeable increase in the expression of immunosuppressive cells in the high AC003092.1 group when compared to the low AC003092.1 group (Figure 6C–6E). Additionally, the tumor microenvironment score, encompassing estimated score, immune score, and stromal score, was significantly elevated in the high AC003092.1 group (Figure 6F–6H). Further exploration of the correlation between AC003092.1 and immunosuppressive checkpoints revealed that immunosuppressive checkpoints (TGFBR1, CTLA4, and CD96) were also significantly upregulated in the high AC003092.1 group (Figure 6I–6K).

AC003092-knockdown suppressed proliferation in Caki-1 and 769-P cells

RT-qPCR results indicated that AC003092.1 was substantially upregulated in ccRCC tissues (Figure 7A). Comparative analysis with HK2 cell lines showed a significant increase in AC003092.1 expression in renal cell lines, particularly in 769-P and Caki-1, with the highest expression observed in Caki-1 (Figure 7B). Subsequently, AC003092.1-shRNA was transfected into

769-P and Caki-1 cells to effectively knock down AC003092.1, confirmed by RT-qPCR (Figure 7C). Next, CCK8 assay revealed that AC003092.1 knockdown led to a reduction in proliferation in both 769-P and Caki-1 cells (Figure 7D). In the clonogenic assay, AC003092.1 knockdown resulted in a significantly lower number of colonies formed in both 769-P and Caki-1 cells compared to the empty vector controls (Figure 7E).

DISCUSSION

Epidemiological studies have revealed a rising incidence and mortality rate of RCC. RCC is characterized as an immunogenic tumor with infiltrating myeloid cell, including macrophages and neutrophils as well as CD8+ T cells and natural killer (NK) cells [23]. Despite the identification of immune cells and immune checkpoints as novel prognostic biomarkers and therapeutic targets for ccRCC, only a fraction of patients with ccRCC benefit from such approaches [9, 24]. The dysregulation of eRNAs is closely linked to various human diseases and immune microenvironment, making eRNAs a promising target for effective therapeutic interventions [25, 26]. Therefore, our objective was to construct a novel IREs prognostic
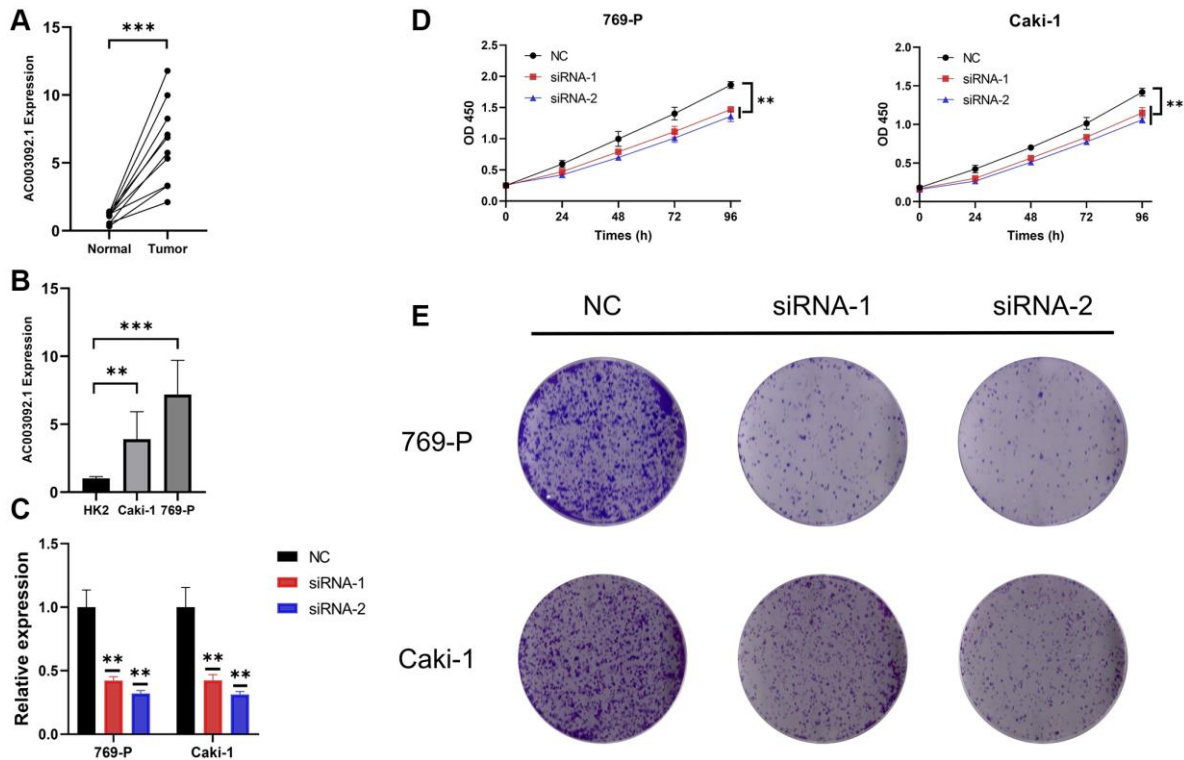

Figure 7. AC003092-knockdown suppressed proliferation in caki-1 and 769-P cells. (**A**) Differences in AC003092.1 expression between ccRCC tissues and adjacent tissues; (**B**) Differences in AC003092.1 expression between HK2 and renal cell lines 769-P and Caki-1; (**C**) The expression of AC003092 was downregulated in 769-P and Caki-1 cells, respectively, as determined by RT-qPCR; (**D**) AC003092-knockdown suppressed ccRCC cell proliferation in 769-P and Caki-1 cells; (**E**) Clonogenic formation in AC003092-knockdown 769-P and Caki-1 cells, along with images of formed clones following control cells for two weeks.

model for ccRCC, aiming to identify reliable predictive and prognostic biomarkers while exploring new immunotherapeutic targets.

eRNA represents a noncoding RNA transcribed by enhancers, facilitating the activation of target genes [27, 28]. These eRNAs not only play a role in regulating the immune response but are also involved in numerous tumorigenic signaling pathways, such as p53 and immune checkpoints, which hold pivotal roles in tumor progression and metastasis [29]. For instance, KLK3 eRNA (KLK3e) selectively enhances the expression of androgen receptor-regulated genes, thereby promoting the proliferation and metastasis of prostate cancer [30]. NET1e is significantly overexpressed in breast cancer and is associated with poor prognosis [17]. As our understanding of eRNA mechanisms deepens, studies have revealed that eRNAs fulfill diverse biological roles in the metastasis and progression of various tumors [31]. Fan et al. constructed an eRNA-related prognostic model in prostate cancer that effectively predicted patient outcomes and explored the immune characteristics of this model [32]. The similarity between our study and other model-based research lies in the fact that both involve clustering key genes, building models, and subsequently analyzing the model's immune, mutation, and prognostic features [33–38]. Notably, our study extended beyond the prognosis and immune characteristics of the IREs signature; we also identified the most relevant eRNA for survival and conducted in-depth analyses of its immune and clinicopathological characteristics.

In our investigation, AC003092.1 emerged as the IRE most strongly associated with survival in ccRCC. AC003092.1 was significantly upregulated in ccRCC and exhibited a close association with poor prognosis and clinicopathological staging. Furthermore, AC003092.1 displayed a significant positive correlation with immunosuppressive cells and immunosuppressive checkpoints, suggesting its potential involvement in shaping an immunosuppressive microenvironment. Notably, Guo et al. demonstrated that AC003092.1 was an IRE, linked to immune cell composition, function, and pathways, possibly contributing to the formation of glioblastoma multiforme (GBM). In GBM patients, AC003092.1 was significantly correlated with poor prognosis and the upregulated expression of its target gene, TFPI2 [39]. AC003092.1's role in GBM involves enhancing the sensitivity of GBM to temozolomide through the mediation of the miR-195/TFPI-2 signaling pathway, impacting patient prognosis. Furthermore, AC003092.1 can counteract the upregulation of TFPI2 expression by miR-195, thus promoting temozolomide-induced apoptosis [40]. These findings highlighted AC003092.1

as a promising molecular target for preventive and therapeutic strategies of ccRCC. However, a comprehensive understanding of the molecular mechanisms governing AC003092.1's aberrant regulation and its role in ccRCC progression necessitates further investigation, ideally through *in vivo* and *in vitro* experimental analysis.

Nonetheless, it is important to acknowledge certain limitations in our study. Firstly, our data analysis relied on publicly available datasets, and additional datasets should be employed for further validation of our results. Additionally, the biological mechanism underlying AC003092.1's influence on reshaping the immunosuppressive microenvironment warrant exploration through in-depth *in vivo* and *in vitro* experiments.

CONCLUSION

IREs played a pivotal role in shaping the immunosuppressive TME in ccRCC. The IREs signature demonstrated remarkable accuracy in distinguishing the immune characteristics and predicting the prognosis of ccRCC patients. AC003092.1, specifically, exhibited an immunosuppressive effect within the TME and hold promise as a potential therapeutic target for ccRCC treatment.

AUTHOR CONTRIBUTIONS

Yang Li and Hongqi Chen designed this work. Lili Niu and Yulin Yue were responsible for the revised and funding. Qiang Li wrote the manuscript. Yang Lv performed the bioinformatics analysis and performed experiments. Wenchuan Shao and Xinghan Yan performed the data review. All authors have read and approved the manuscript.

CONFLICTS OF INTEREST

The authors declare no conflicts of interest related to this study.

ETHICAL STATEMENT

The protocols for cell experiments adhered to established ethical guidelines and standards for cellular research. We understand the importance of ethical considerations in scientific research and confirm that our study was conducted in accordance with the relevant ethical guidelines.

FUNDING

REFERENCES

1. Shuch B, Amin A, Armstrong AJ, Eble JN, Ficarra V, Lopez-Beltran A, Martignoni G, Rini BI, Kutikov A. Understanding pathologic variants of renal cell carcinoma: distilling therapeutic opportunities from biologic complexity. Eur Urol. 2015; 67:85–97.
https://doi.org/10.1016/j.eururo.2014.04.029
PMID:24857407

2. Barata PC, Rini BI. Treatment of renal cell carcinoma: Current status and future directions. CA Cancer J Clin. 2017; 67:507–24.
https://doi.org/10.3322/caac.21411
PMID:28961310

3. Ljungberg B, Bensalah K, Canfield S, Dabestani S, Hofmann F, Hora M, Kuczyk MA, Lam T, Marconi L, Merseburger AS, Mulders P, Powles T, Staehler M, et al. EAU guidelines on renal cell carcinoma: 2014 update. Eur Urol. 2015; 67:913–24.
https://doi.org/10.1016/j.eururo.2015.01.005
PMID:25616710

4. Escudier B, Porta C, Schmidinger M, Rioux-Leclercq N, Bex A, Khoo V, Grünwald V, Gillessen S, Horwich A, and ESMO Guidelines Committee. Renal cell carcinoma: ESMO Clinical Practice Guidelines for diagnosis, treatment and follow-up†. Ann Oncol. 2019; 30:706–20.
https://doi.org/10.1093/annonc/mdz056
PMID:30788497

5. Hsieh JJ, Purdue MP, Signoretti S, Swanton C, Albiges L, Schmidinger M, Heng DY, Larkin J, Ficarra V. Renal cell carcinoma. Nat Rev Dis Primers. 2017; 3:17009.
https://doi.org/10.1038/nrdp.2017.9
PMID:28276433

6. Bray F, Ferlay J, Soerjomataram I, Siegel RL, Torre LA, Jemal A. Global cancer statistics 2018: GLOBOCAN estimates of incidence and mortality worldwide for 36 cancers in 185 countries. CA Cancer J Clin. 2018; 68:394–424.
https://doi.org/10.3322/caac.21492
PMID:30207593

7. Díaz-Montero CM, Rini BI, Finke JH. The immunology of renal cell carcinoma. Nat Rev Nephrol. 2020; 16:721–35.
https://doi.org/10.1038/s41581-020-0316-3
PMID:32733094

8. Giraldo NA, Becht E, Vano Y, Petitprez F, Lacroix L, Validire P, Sanchez-Salas R, Ingels A, Oudard S, Moatti A, Buttard B, Bourass S, Germain C, et al. Tumor-Infiltrating and Peripheral Blood T-cell Immunophenotypes Predict Early Relapse in Localized Clear Cell Renal Cell Carcinoma. Clin Cancer Res. 2017; 23:4416–28.
https://doi.org/10.1158/1078-0432.CCR-16-2848
PMID:28213366

9. Blankenstein T, Coulie PG, Gilboa E, Jaffee EM. The determinants of tumour immunogenicity. Nat Rev Cancer. 2012; 12:307–13.
https://doi.org/10.1038/nrc3246
PMID:22378190

10. Cella D, Grünwald V, Escudier B, Hammers HJ, George S, Nathan P, Grimm MO, Rini BI, Doan J, Ivanescu C, Paty J, Mekan S, Motzer RJ. Patient-reported outcomes of patients with advanced renal cell carcinoma treated with nivolumab plus ipilimumab versus sunitinib (CheckMate 214): a randomised, phase 3 trial. Lancet Oncol. 2019; 20:297–310.
https://doi.org/10.1016/S1470-2045(18)30778-2
PMID:30658932

11. Guttman M, Rinn JL. Modular regulatory principles of large non-coding RNAs. Nature. 2012; 482:339–46.
https://doi.org/10.1038/nature10887
PMID:22337053

12. Lin W, Zhou Q, Wang CQ, Zhu L, Bi C, Zhang S, Wang X, Jin H. LncRNAs regulate metabolism in cancer. Int J Biol Sci. 2020; 16:1194–206.
https://doi.org/10.7150/ijbs.40769
PMID:32174794

13. Liang Y, Chen X, Wu Y, Li J, Zhang S, Wang K, Guan X, Yang K, Bai Y. LncRNA CASC9 promotes esophageal squamous cell carcinoma metastasis through upregulating LAMC2 expression by interacting with the CREB-binding protein. Cell Death Differ. 2018; 25:1980–95.
https://doi.org/10.1038/s41418-018-0084-9
PMID:29511340

14. Bhan A, Soleimani M, Mandal SS. Long Noncoding RNA and Cancer: A New Paradigm. Cancer Res. 2017; 77:3965–81.
https://doi.org/10.1158/0008-5472.CAN-16-2634
PMID:28701486

15. Li W, Notani D, Rosenfeld MG. Enhancers as non-coding RNA transcription units: recent insights and future perspectives. Nat Rev Genet. 2016; 17:207–23.
https://doi.org/10.1038/nrg.2016.4
PMID:26948815

16. Huang J, Wang J, He H, Huang Z, Wu S, Chen C, Liu W, Xie L, Tao Y, Cong L, Jiang Y. Close interactions between lncRNAs, lipid metabolism and ferroptosis in cancer. Int J Biol Sci. 2021; 17:4493–513.
https://doi.org/10.7150/ijbs.66181

PMID:34803512

17. Zhang Z, Lee JH, Ruan H, Ye Y, Krakowiak J, Hu Q, Xiang Y, Gong J, Zhou B, Wang L, Lin C, Diao L, Mills GB, et al. Transcriptional landscape and clinical utility of enhancer RNAs for eRNA-targeted therapy in cancer. Nat Commun. 2019; 10:4562.
https://doi.org/10.1038/s41467-019-12543-5
PMID:31594934

18. Peng WX, Koirala P, Mo YY. LncRNA-mediated regulation of cell signaling in cancer. Oncogene. 2017; 36:5661–7.
https://doi.org/10.1038/onc.2017.184
PMID:28604750

19. Tan SH, Leong WZ, Ngoc PCT, Tan TK, Bertulfo FC, Lim MC, An O, Li Z, Yeoh AEJ, Fullwood MJ, Tenen DG, Sanda T. The enhancer RNA *ARIEL* activates the oncogenic transcriptional program in T-cell acute lymphoblastic leukemia. Blood. 2019; 134:239–51.
https://doi.org/10.1182/blood.2018874503
PMID:31076442

20. Napoli S, Munz N, Guidetti F, Bertoni F. Enhancer RNAs (eRNAs) in Cancer: The Jacks of All Trades. Cancers (Basel). 2022; 14:1978.
https://doi.org/10.3390/cancers14081978
PMID:35454885

21. Murakami S, Gadad SS, Kraus WL. A PreSTIGEous use of LncRNAs to predict enhancers. Cell Cycle. 2015; 14:1619–20.
https://doi.org/10.1080/15384101.2015.1032650
PMID:25928187

22. Gu X, Wang L, Boldrup L, Coates PJ, Fahraeus R, Sgaramella N, Wilms T, Nylander K. *AP001056.1*, A Prognosis-Related Enhancer RNA in Squamous Cell Carcinoma of the Head and Neck. Cancers (Basel). 2019; 11:347.
https://doi.org/10.3390/cancers11030347
PMID:30862109

23. Komohara Y, Hasita H, Ohnishi K, Fujiwara Y, Suzu S, Eto M, Takeya M. Macrophage infiltration and its prognostic relevance in clear cell renal cell carcinoma. Cancer Sci. 2011; 102:1424–31.
https://doi.org/10.1111/j.1349-7006.2011.01945.x
PMID:21453387

24. Nakano O, Sato M, Naito Y, Suzuki K, Orikasa S, Aizawa M, Suzuki Y, Shintaku I, Nagura H, Ohtani H. Proliferative activity of intratumoral CD8(+) T-lymphocytes as a prognostic factor in human renal cell carcinoma: clinicopathologic demonstration of antitumor immunity. Cancer Res. 2001; 61:5132–6.
PMID:11431351

25. Arnold PR, Wells AD, Li XC. Diversity and Emerging Roles of Enhancer RNA in Regulation of Gene Expression and Cell Fate. Front Cell Dev Biol. 2020; 7:377.
https://doi.org/10.3389/fcell.2019.00377
PMID:31993419

26. Léveillé N, Melo CA, Agami R. Enhancer-associated RNAs as therapeutic targets. Expert Opin Biol Ther. 2015; 15:723–34.
https://doi.org/10.1517/14712598.2015.1029452
PMID:25819025

27. Kim TK, Hemberg M, Gray JM, Costa AM, Bear DM, Wu J, Harmin DA, Laptewicz M, Barbara-Haley K, Kuersten S, Markenscoff-Papadimitriou E, Kuhl D, Bito H, et al. Widespread transcription at neuronal activity-regulated enhancers. Nature. 2010; 465:182–7.
https://doi.org/10.1038/nature09033
PMID:20393465

28. Sartorelli V, Lauberth SM. Enhancer RNAs are an important regulatory layer of the epigenome. Nat Struct Mol Biol. 2020; 27:521–8.
https://doi.org/10.1038/s41594-020-0446-0
PMID:32514177

29. Melo CA, Drost J, Wijchers PJ, van de Werken H, de Wit E, Oude Vrielink JA, Elkon R, Melo SA, Léveillé N, Kalluri R, de Laat W, Agami R. eRNAs are required for p53-dependent enhancer activity and gene transcription. Mol Cell. 2013; 49:524–35.
https://doi.org/10.1016/j.molcel.2012.11.021
PMID:23273978

30. Hsieh CL, Fei T, Chen Y, Li T, Gao Y, Wang X, Sun T, Sweeney CJ, Lee GS, Chen S, Balk SP, Liu XS, Brown M, Kantoff PW. Enhancer RNAs participate in androgen receptor-driven looping that selectively enhances gene activation. Proc Natl Acad Sci U S A. 2014; 111:7319–24.
https://doi.org/10.1073/pnas.1324151111
PMID:24778216

31. Cai S, Hu X, Chen R, Zhang Y. Identification and Validation of an Immune-Related eRNA Prognostic Signature for Hepatocellular Carcinoma. Front Genet. 2021; 12:657051.
https://doi.org/10.3389/fgene.2021.657051
PMID:34178028

32. Fan S, Wang Z, Zhao L, Zhao C, Yuan D, Wang J. A Robust Prognostic Gene Signature Based on eRNAs-Driven Genes in Prostate Cancer. Front Genet. 2021; 12:676845.
https://doi.org/10.3389/fgene.2021.676845
PMID:34267780

33. Gao C, Zhang R, Chen X, Yao T, Song Q, Ye W, Li P, Wang Z, Yi D, Wu Y. Integrating Internet multisource big data to predict the occurrence and development of COVID-19 cryptic transmission. NPJ Digit Med.

2022; 5:161.
https://doi.org/10.1038/s41746-022-00704-8
PMID:36307547

34. Lai G, Zhong X, Liu H, Deng J, Li K, Xie B. Development of a Hallmark Pathway-Related Gene Signature Associated with Immune Response for Lower Grade Gliomas. Int J Mol Sci. 2022; 23:11971.
https://doi.org/10.3390/ijms231911971
PMID:36233273

35. Lai G, Zhong X, Liu H, Deng J, Li K, Xie B. A Novel m7G-Related Genes-Based Signature with Prognostic Value and Predictive Ability to Select Patients Responsive to Personalized Treatment Strategies in Bladder Cancer. Cancers (Basel). 2022; 14:5346.
https://doi.org/10.3390/cancers14215346
PMID:36358764

36. Lai G, Liu H, Deng J, Li K, Zhang C, Zhong X, Xie B. The Characteristics of Tumor Microenvironment Predict Survival and Response to Immunotherapy in Adrenocortical Carcinomas. Cells. 2023; 12:755.
https://doi.org/10.3390/cells12050755
PMID:36899891

37. Lai G, Liu H, Deng J, Li K, Xie B. A Novel 3-Gene Signature for Identifying COVID-19 Patients Based on Bioinformatics and Machine Learning. Genes (Basel). 2022; 13:1602.
https://doi.org/10.3390/genes13091602
PMID:36140771

38. Ma Q, Tao H, Li Q, Zhai Z, Zhang X, Lin Z, Kuang N, Pan J. OrganoidDB: a comprehensive organoid database for the multi-perspective exploration of bulk and single-cell transcriptomic profiles of organoids. Nucleic Acids Res. 2023; 51:D1086–93.
https://doi.org/10.1093/nar/gkac942
PMID:36271792

39. Guo XY, Zhong S, Wang ZN, Xie T, Duan H, Zhang JY, Zhang GH, Liang L, Cui R, Hu HR, Lu J, Wu Y, Dong JJ, et al. Immunogenomic Profiling Demonstrate AC003092.1 as an Immune-Related eRNA in Glioblastoma Multiforme. Front Genet. 2021; 12:633812.
https://doi.org/10.3389/fgene.2021.633812
PMID:33815468

40. Xu N, Liu B, Lian C, Doycheva DM, Fu Z, Liu Y, Zhou J, He Z, Yang Z, Huang Q, Zeng H, Guo H. Long noncoding RNA AC003092.1 promotes temozolomide chemosensitivity through miR-195/TFPI-2 signaling modulation in glioblastoma. Cell Death Dis. 2018; 9:1139.
https://doi.org/10.1038/s41419-018-1183-8
PMID:30442884

SUPPLEMENTARY MATERIALS

Supplementary Figure
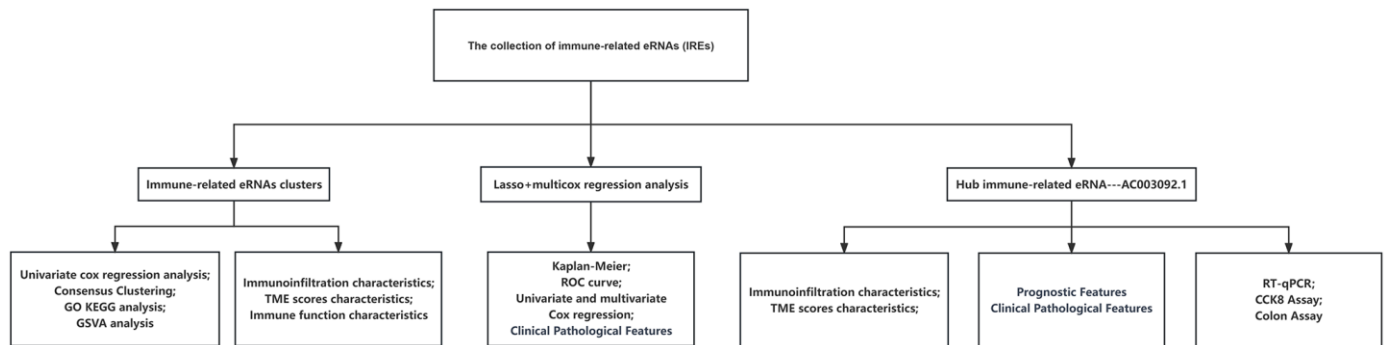
Supplementary Figure 1. The flow chart of the research.

Supplementary Tables

Please browse Full Text version to see the data of Supplementary Table 1.

Supplementary Table 1. Univariate Cox regression analysis results of IREs.

Supplementary Table 2. Prognostic features of IREs and correlation of target genes.

eRNA	KM	Target	cor	cor*P*val
AC003092.1	8.82E-08	TFPI2	0.522450477	4.42E-39
EMX2OS	6.02E-07	EMX2	0.809246934	0
CCDC18-AS1	7.21E-06	CCDC18	0.74912757	0
LINC01389	2.27E-05	FOXD2	0.418684344	2.74E-24
STX4	3.93E-05	FBXL19	0.625144013	0
STX4	3.93E-05	HSD3B7	0.626346923	0
STX4	3.93E-05	ORAI3	0.556775018	0
STX4	3.93E-05	PRSS53	0.650196372	0
SSPO	0.000113124	ZNF467	0.42944313	0
SSPO	0.000113124	ZNF862	0.678603729	0
SLC25A24P1	0.000144688	NBPF4	0.523680588	2.74E-39
SLC25A24P1	0.000144688	NBPF6	0.485813742	2.86E-33
FRY	0.000161361	FRY	1	0
AFG3L1P	0.000331435	FANCA	0.417693895	0
AFG3L1P	0.000331435	MC1R	0.786988388	0
AFG3L1P	0.000331435	SPIRE2	0.424867444	0
AFG3L1P	0.000331435	AFG3L1P	1	0
LINC00671	0.000426575	G6PC	0.703641148	9.92E-82
SPAAR	0.000479272	RECK	0.541849696	1.87E-42
HOTAIR	0.000480838	HOXC11	0.691390398	7.69E-78
HOTAIR	0.000480838	HOXC13	0.411470753	1.94E-23
HOTAIR	0.000480838	HOXC6	0.479131856	2.77E-32
LINC01176	0.00056786	NOD1	0.435177939	2.58E-26
HAGLR	0.001295545	HOXD1	0.855324249	1.74E-155
HAGLR	0.001295545	HOXD3	0.624327104	0
HAGLR	0.001295545	HOXD4	0.729164875	0
HAGLR	0.001295545	HOXD8	0.510689552	0
RASGEF1B	0.001866563	RASGEF1B	1	0
AP001189.3	0.001936226	LRRC32	0.819526937	5.87E-132
RSRP1	0.002838905	RHD	0.448506225	4.93E-28
ZNF337-AS1	0.02853277	NINL	0.521776524	0
ZNF337-AS1	0.02853277	ZNF337	0.607919036	0